Supporting Information

Improved performance of organic single-crystal thin-film transistors via contact doping with a high electron-affinity dopant

Xinmin Shi,[a] Wei Deng,*[b] Shiquan He,[b] Xiaobin Ren,[b] Haoyu Jiang,[b] Yuqing Luo,[a] Bo Zhao,[a] Xiujuan Zhang *[b] and Jiansheng Jie *[ab]

[a]Macao Institute of Materials Science and Engineering (MIMSE)
MUST-SUDA Joint Research Center for Advanced Functional Materials
Macau University of Science and Technology
Taipa, Macau SAR 999078, China

[b]State Key Laboratory of Bioinspired Interfacial Materials Science
Institute of Functional Nano & Soft Materials (FUNSOM)
Soochow University
Suzhou, Jiangsu 215123, China

*Corresponding authors: Jiansheng Jie (jsjie@suda.edu.cn), Wei Deng (dengwei@suda.edu.cn) and Xiujuan Zhang (xjzhang@suda.edu.cn)

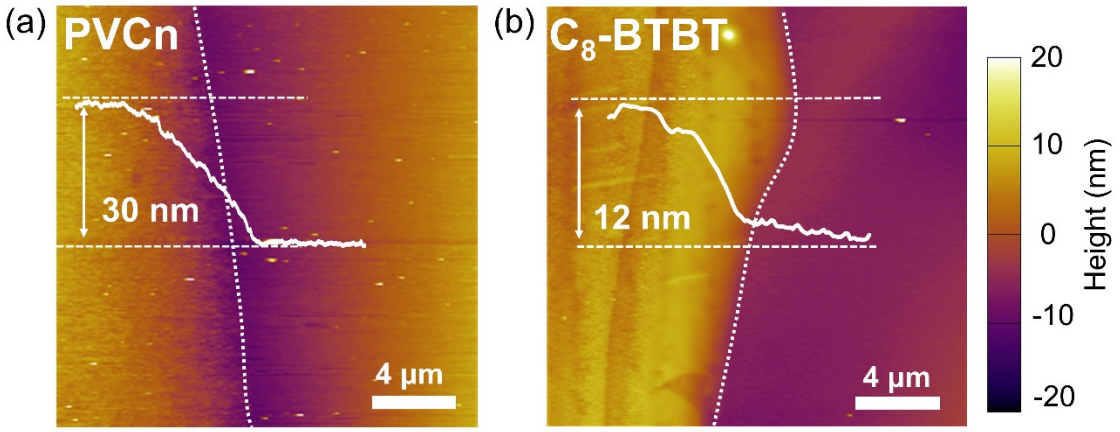

Figure S1. AFM height images and corresponding line profiles of the step structures used for thickness determination. (a) PVCn film deposited on SiO_2, where the right region corresponds to the exposed SiO_2 surface and the left region corresponds to the PVCn film. (b) C_8-BTBT film on SiO_2, where the right region corresponds to the exposed SiO_2 surface and the left region corresponds to the C_8-BTBT film.

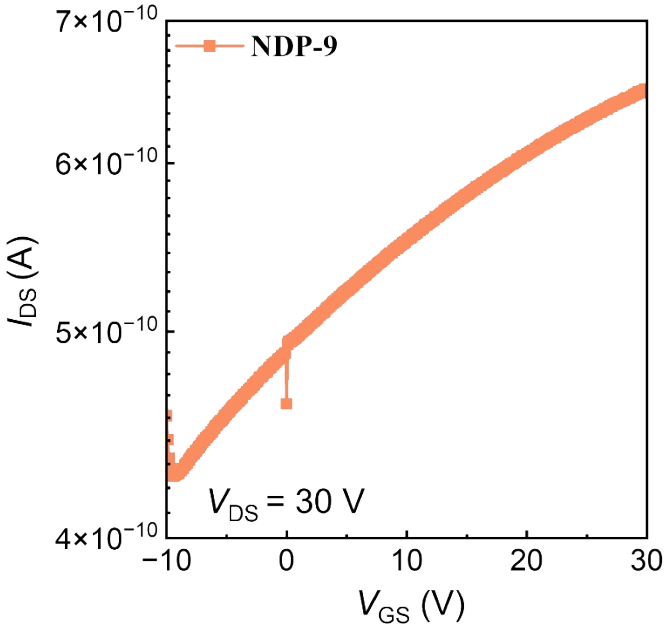

Figure S2. Transfer characteristics of the NDP-9-based transistor.

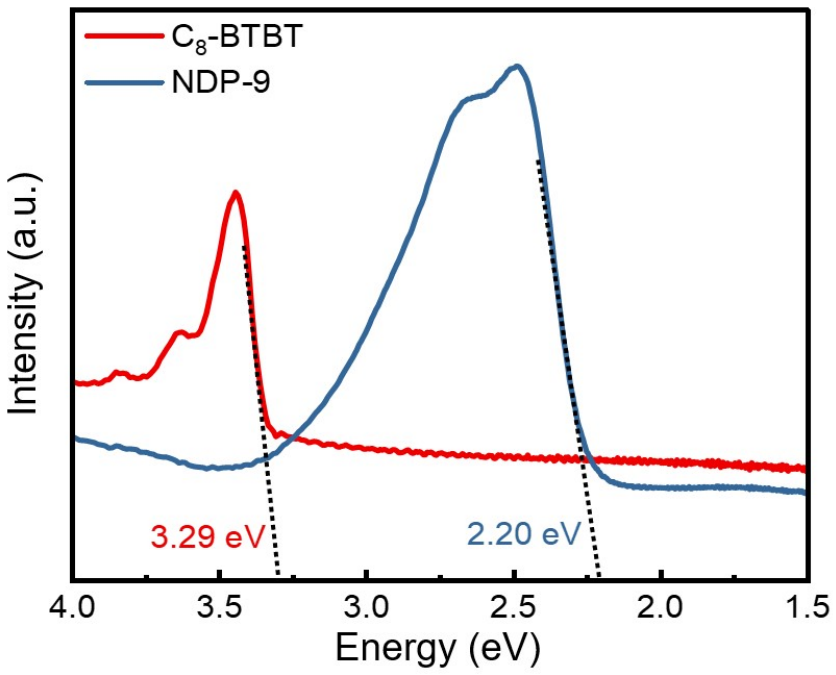

Figure S3. UV-Vis-NIR, the optical gap of NDP-9 is about 2.22 eV.

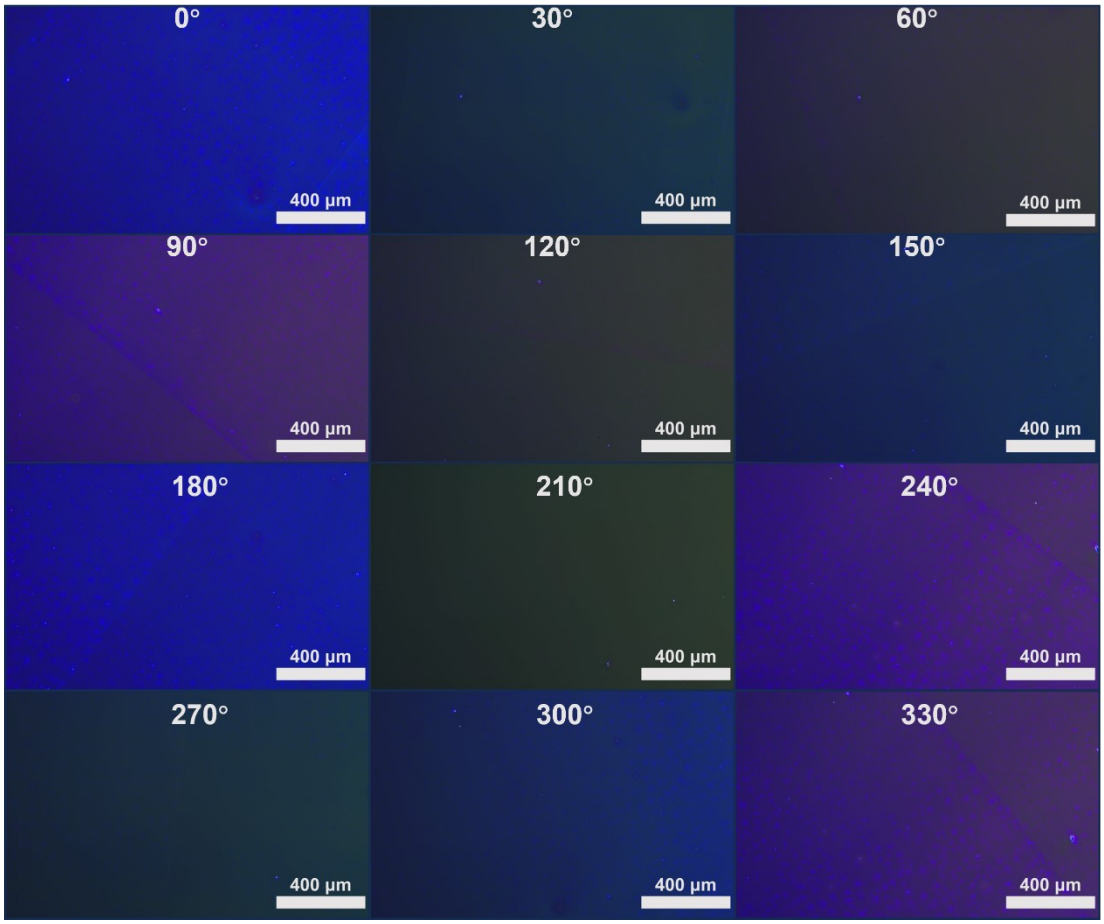

Figure S4. Orientation characterization. POM images of C_8-BTBT OSCF captured under different polarization angles 0-360°.

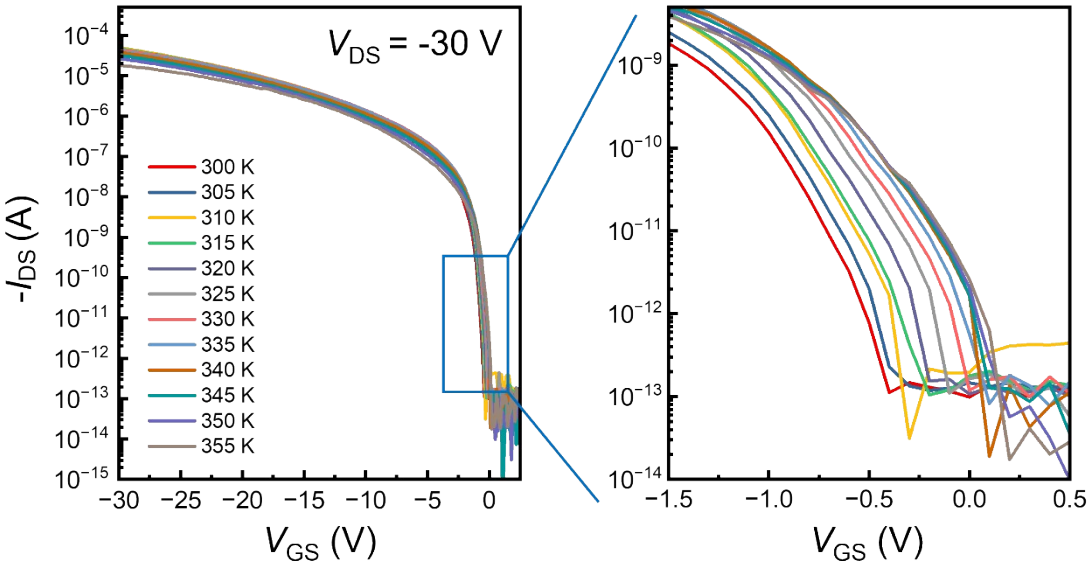

Figure S5. Transfer curves at different temperatures from 300 to 355 K.

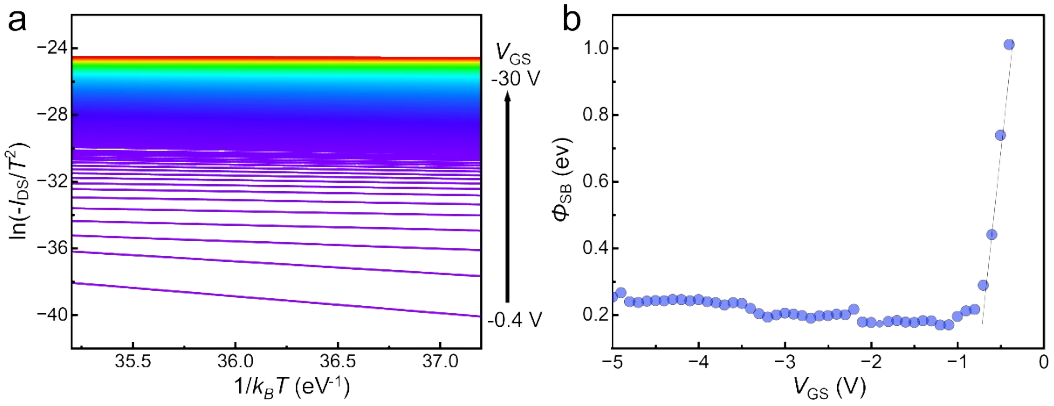

Figure S6. (a) The transfer curves under different temperature of the Schottky barrier OFET without the NDP-9 layer, V_{DS} = -30 V. (b) The linear fitting results of $\ln(I_{DS}/T^2)$ versus $1/k_BT$ under different V_{GS}.

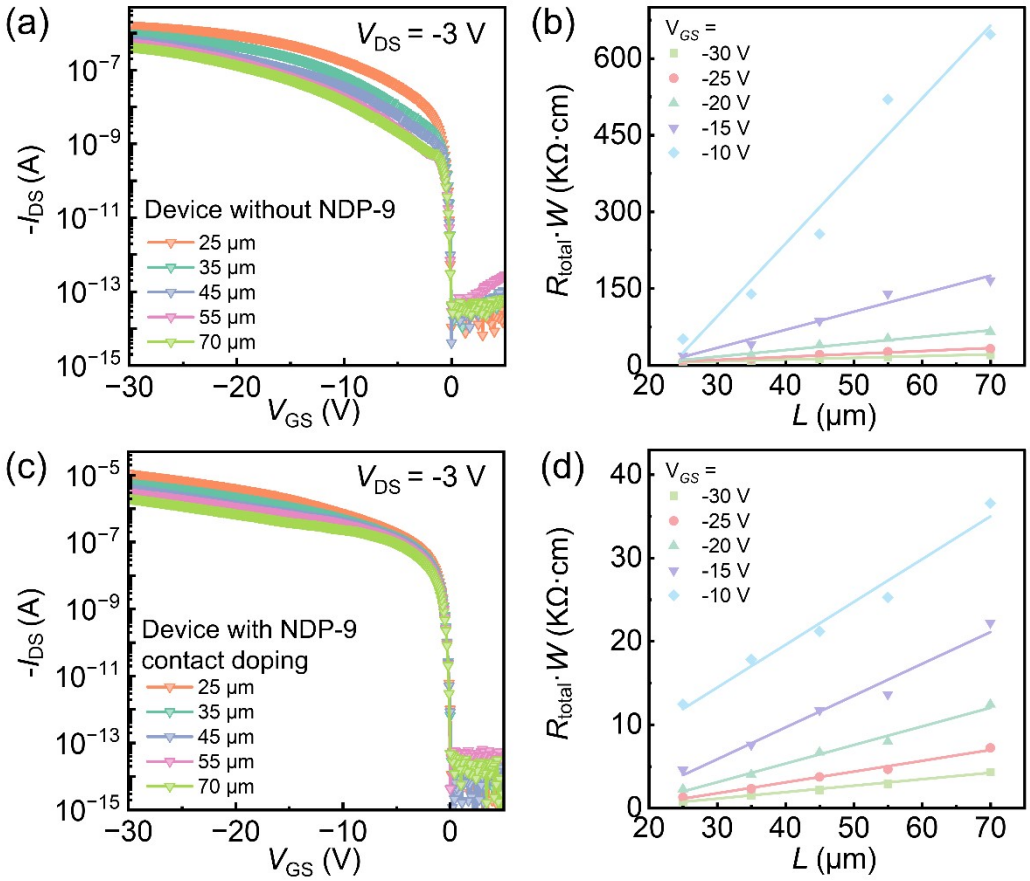

Figure S7. Transmission line method (TLM) analysis of OTFTs with and without an NDP-9 interlayer (a) Transfer characteristics of devices without NDP-9 measured at V_{DS} = -3 V with different channel lengths. (b) Total resistance normalized by channel width ($R_{total} \cdot W$) as a function of channel length for devices without NDP-9 at different V_{GS}. (c) Transfer characteristics of devices with NDP-9 contact doping measured at V_{DS} = -3 V with different channel lengths. (d) Total resistance normalized by channel width ($R_{total} \cdot W$) as a function of channel length for devices with NDP-9 contact doping at different V_{GS}.

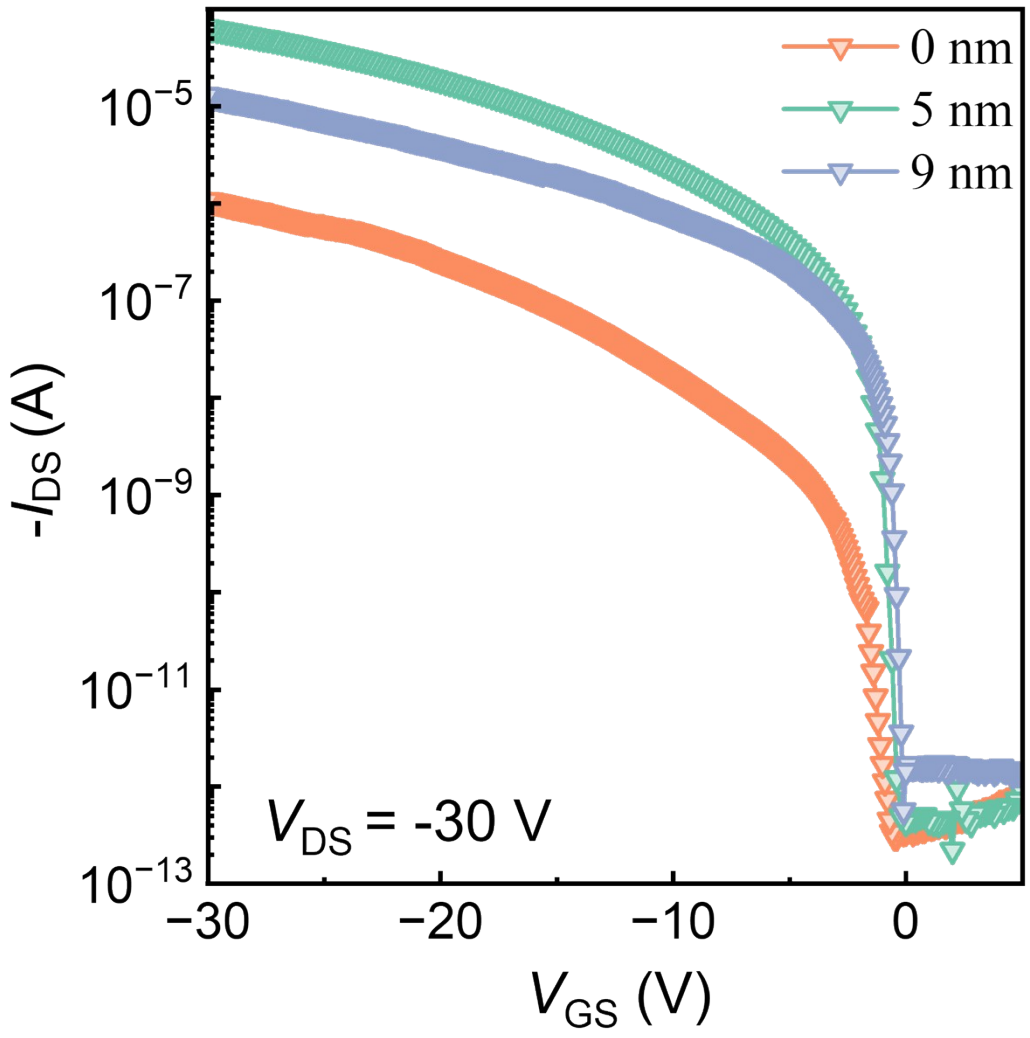

Figure S8. Transfer characteristics of OTFTs with different NDP-9 interlayer thicknesses (0, 5, and 9 nm) measured at V_{DS} = -30 V.

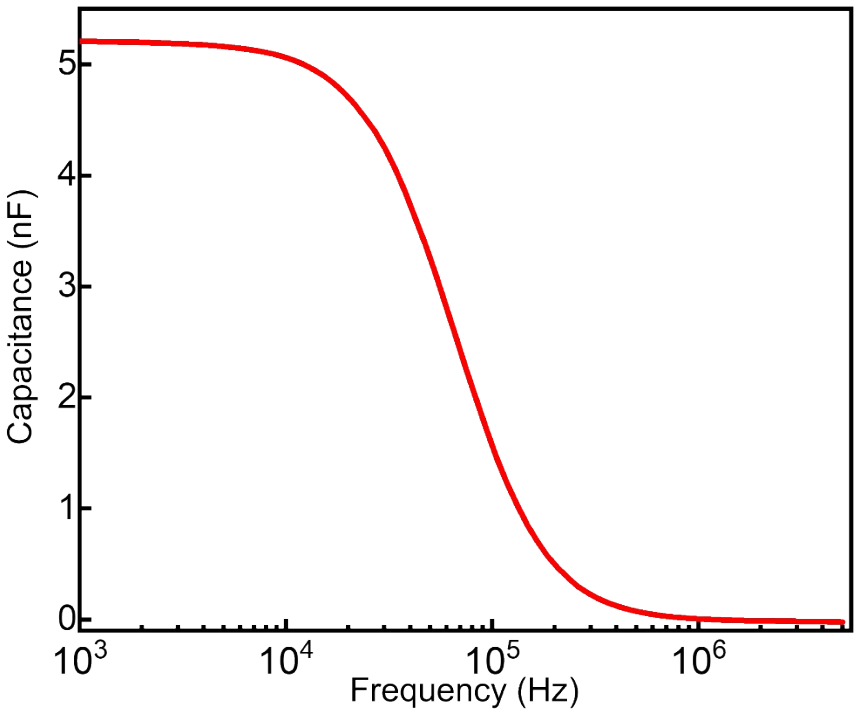

Figure S9. Capacity measurement of the PVC_n and SiO_2 double-layer insulator.

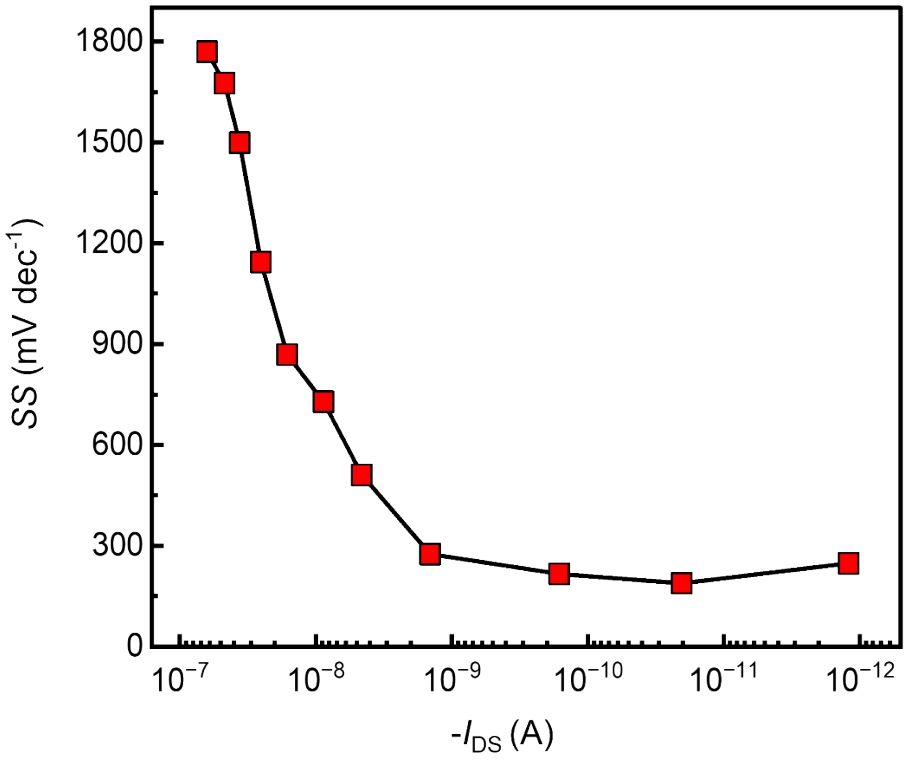

Figure S10. Subthreshold swing versus I_{DS} extracted from the transfer curve of the OSC-TFT with NDP-9 contact doping.

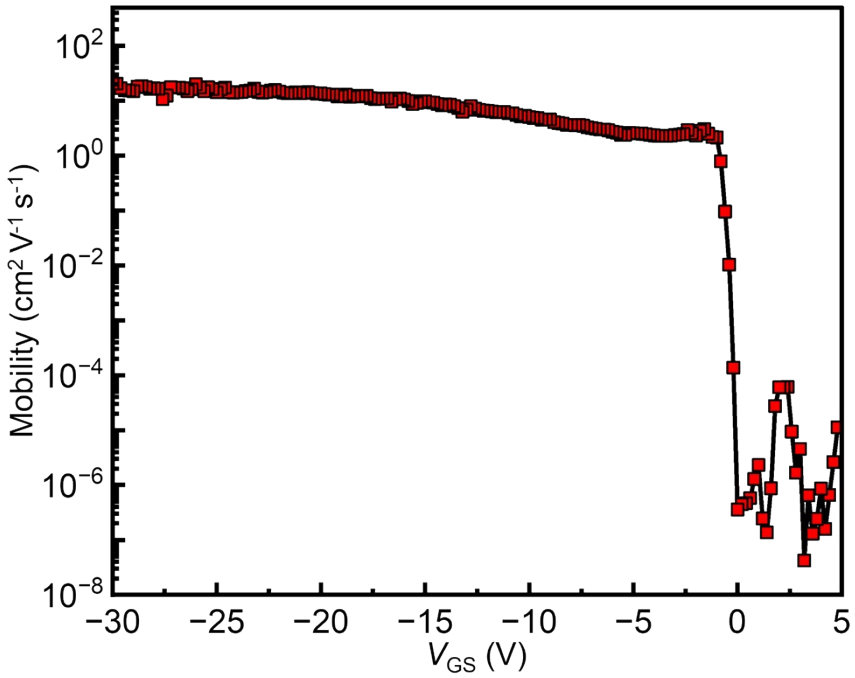

Figure S11. Mobility as a function of gate voltage in the OTFT with NDP-9 contact doping.

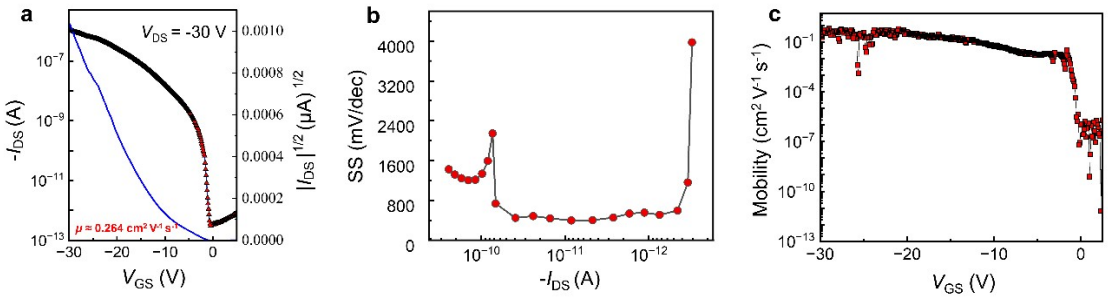

Figure S12. (a) Saturation region transfer. (b) I_{DS}-*SS*.(c) Mobility as a function of gate voltage in the OSC-TFT without NDP-9 contact doping.

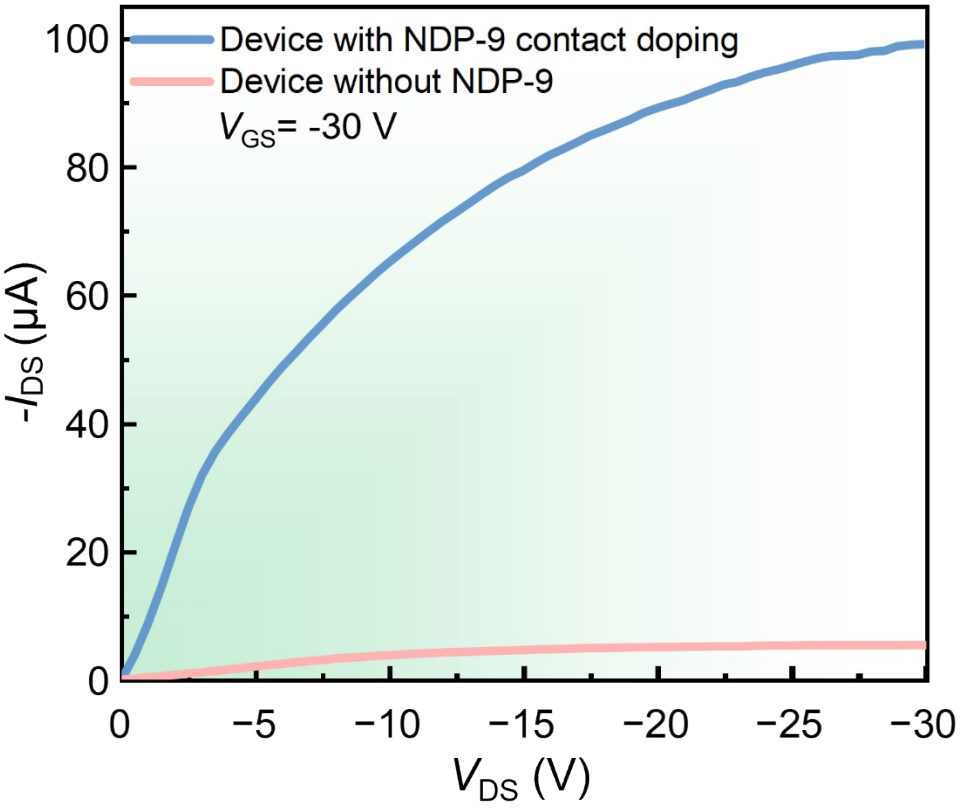

Figure S13. Output characteristics of OTFTs measured at V_{GS} = -30 V, with (blue) and without (red) the NDP-9 interlayer. The NDP-9 device shows higher current and reduced nonlinearity.

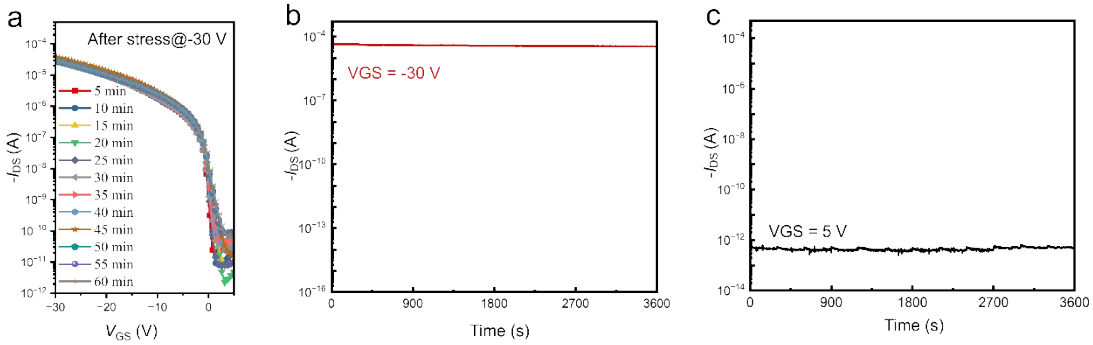

Figure S14. Bias-stress stability of NDP-9 contact-doped OTFTs.